The Virtual Element Method for a Minimal Surface Problem

P. F. Antonietti[1], S. Bertoluzza[2], D. Prada[3], and M. Verani[4]

[1] MOX, Dipartimento di Matematica, Politecnico di Milano, Italy; *e-mail: paola.antonietti@polimi.it*
[2]Istituto di Matematica Applicata e Tecnologie Informatiche - CNR, Pavia, Italy *e-mail: silvia.bertoluzza@imati.cnr.it*
[3]Istituto di Matematica Applicata e Tecnologie Informatiche - CNR, Pavia, Italy *e-mail: daniele.prada@imati.cnr.it*
[4] MOX, Dipartimento di Matematica, Politecnico di Milano, Italy and Istituto di Matematica Applicata e Tecnologie Informatiche - CNR, Pavia, Italy
e-mail: marco.verani@polimi.it

December 23, 2019

Abstract

In this paper we consider the Virtual Element discretization of a minimal surface problem, a quasi-linear elliptic partial differential equation modeling the problem of minimizing the area of a surface subject to a prescribed boundary condition. We derive optimal error estimate and present several numerical tests assessing the validity of the theoretical results.

1 Introduction

In recent years, the numerical approximation of partial differential equations on computational meshes composed by arbitrarily-shaped polygonal/polyhedral (polytopal, for short) elements has been the subject of an intense research activity. Examples of such methods include the Mimetic Finite Difference method, the Polygonal Finite Element Method, the polygonal Discontinuous Galerkin Finite Element Methods, the Hybridizable Discontinuous Galerkin and Hybrid High-Order Methods, the Gradient Discretization method, the Finite Volume Method, the BEM-based FEM, the Weak Galerkin method and the Virtual Element method (VEM). For more details see the special issue [6] and the references therein. VEM has been introduced in [10] for elliptic problems and later

extended to several different linear and non-linear differential problems. While the analysis of linear problems is much more flourished, the study of Virtual Element discretization for non-linear problems is much less developed (see, e.g., [4, 15, 11, 9, 5, 7, 12, 20, 3, 2, 1, 17]). In this paper we contribute to fill this gap by addressing the (lowest order) Virtual Element discretization of a minimal surface problem (see, e.g., [13] for its finite element discretization). More precisely, in Section 2 we introduce the continuous problem together with its Virtual Element discretization, while in Section 3 we derive optimal error estimate in the H^1-norm, under a condition on the discrete solution, the validity of which can be checked "a posteriori". Finally, in Section 4 we present several numerical results assessing the validity of the theoretical estimate and confirming that optimal convergence is indeed achieved. Moreover, the convergence properties in the L^2-norm is numerically investigated.

1.1 Notation

Throughout the paper we shall use the standard notation of the Sobolev spaces $H^m(\mathcal{D})$ for a nonnegative integer m and an open bounded domain $\mathcal{D}$. The m-th seminorm of the function v will be denoted by

$$|v|^2_{m,\mathcal{D}} = \sum_{|\alpha|=m} \left\| \frac{\partial^{|\alpha|} v}{\partial_{x_1}^{\alpha_1} \partial_{x_2}^{\alpha_2}} \right\|^2_{0,\mathcal{D}},$$

where $\|\cdot\|_{0,\mathcal{D}}$ stands for the $L^2(\mathcal{D})$ norm and we set $|\alpha| = \alpha_1 + \alpha_2$ for the nonnegative multi-index $\alpha = (\alpha_1, \alpha_2)$. For any integer $m \geq 0$, $\mathbb{P}^m(\mathcal{D})$ is the space of polynomials of total degree up to m defined on $\mathcal{D}$. Moreover, $n = (n_1, n_2)$ is the outward unit normal vector to $\partial\mathcal{D}$, the boundary of $\mathcal{D}$. Finally, we will employ the symbol $\lesssim$ for an inequality holding up to a constant independent of the mesh size.

2 Continuous problem and its VEM discretization

Let $\Omega \subseteq \mathbb{R}^2$ be a bounded open set. In the following, we will employ the following notation

$$f(\cdot) = \sqrt{1 + |\nabla(\cdot)|^2}.$$

Let φ be a function given on the boundary $\Gamma = \partial\Omega$. The minimal surface problem amounts to finding a function u which minimizes the functional

$$J(v) = \int_\Omega f(v) dx$$

over a suitable space of functions which are equal to φ on Γ. The existence and uniqueness of a solution is a delicate mathematical issue (see, e.g., [13] and the references therein). Here, with the aim of simplifying the analysis, we follow

the framework considered, e.g., in [13] and make the following hypotheses: the domain Ω is a convex polygonal set and the function φ is the trace over Γ of a function (by abuse of notation still denoted by φ) of $H^2(\Omega)$. Moreover, for the subsequent discussion, as in [13], we consider that the minimal surface problem consists in solving the following:

$$u = \arg\min_{v \in V^\varphi} J(v), \tag{1}$$

where $V^\varphi = \{v \in H^1(\Omega) : \ u = \varphi \text{ on } \partial\Omega\}$. Note that u is the solution to (1) if and only if $u \in V^\varphi$ solves

$$\int_\Omega \frac{\nabla u \cdot \nabla v}{f(u)} = 0 \qquad \forall v \in V^0 = H_0^1(\Omega). \tag{2}$$

Let $\{\mathcal{T}_h\}_h$ be a sequence of decompositions (meshes) of Ω into non-overlapping polygons E. Each mesh $\mathcal{T}_h$ is labeled by the mesh size parameter h, which will be defined below, and satisfies suitable regularity assumptions that are customarily made to prove the convergence of the method and derive an estimate of the approximation error. These regularity assumptions are introduced and discussed in Section 3. Let $\mathcal{E}_h$ be the set of edges of $\mathcal{T}_h$ such that $\mathcal{E}_h = \mathcal{E}_h^i \cup \mathcal{E}_h^\Gamma$, where $\mathcal{E}_h^i$ and $\mathcal{E}_h^\Gamma$ are the set of interior and boundary edges, respectively. Similarly, we denote by $V_h = V_h^i \cup V_h^\Gamma$ the set of vertices in $\mathcal{T}_h$, where V_h^i and V_h^Γ are the sets of interior and boundary vertices, respectively. Accordingly, V_h^E is the set of vertices of E. Moreover, $|E|$ and $|e|$ denote the area of cell E and the length of edge e, respectively, ∂E is the boundary of E, h_E is the diameter of E and the mesh size parameter is defined as $h = \max_{E \in \mathcal{T}_h} h_E$.

Let us introduce the usual local lowest order conforming Virtual Element space on the polygon E (see, e.g., [10])

$$V_h^E = \{v_h \in H^1(E) : \ \Delta v_h = 0 \text{ in } E, \ v_h \in C^0(\partial E), v_h|_e \in \mathbb{P}^1(e) \ \forall e \in \partial E\},$$

where, for D d-dimensional domain, $\mathbb{P}^1(D)$ denotes the space of d-variate polynomials of order less than or equal to one on D. Accordingly, the global Virtual Element space is defined as follows

$$V_h^\varphi = \{v_h \in H^1(\Omega) : \ v_h|_E \in V_h^E, \ v_h(V) = \varphi(V) \ \text{ for each vertex V} \in V_h^\Gamma\}.$$

Consistently, we denote by V_h^0 the global VEM space with homogeneous Dirichlet boundary conditions.

Let $S^E(\cdot,\cdot)$ be the usual stabilization term employed for constructing the VEM discretization of the Laplace problem, i.e. the Euclidean scalar product associated with the degrees of freedom (here the vertex values). See, e.g., [10, 8] for further details. Moreover, let $\Pi_E^\nabla : V_h^E \to \mathbb{P}^1(E)$ the usual elliptic projection operator (see, e.g., [10]).

We introduce the local discrete function $f_h^E : V_h^E \to \mathbb{R}$ defined as

$$f_h^E(v_h) = \sqrt{1 + |\nabla \Pi_E^\nabla v_h|^2 + |E|^{-1} S^E((I - \Pi_E^\nabla)v_h, (I - \Pi_E^\nabla)v_h)}. \tag{3}$$

Roughly speaking, $f_h^E(\cdot)$ represents an approximation to $\sqrt{1+|(\nabla\cdot)_{|E}|^2}$.

Having in mind the above definitions, the discrete virtual counterpart of the continuous minimization problem (1) reads as follows

$$u_h = \arg\min_{v_h \in V_h^\varphi} J_h(v_h), \qquad \text{with} \qquad J_h(v_h) = \sum_{E\in\mathcal{T}_h} \int_E f_h^E(v_h)\, dx. \tag{4}$$

Thus, the Virtual Element discretization of (2) is as follows: find $u_h \in V_h^\varphi$ such that

$$A_h(u_h; u_h, v_h) = 0 \tag{5}$$

for all $v_h \in V_h^0$, where $A_h(w_h; u_h, v_h) = \sum_E A_h^E(w_h; u_h, v_h)$ and

$$A_h^E(w_h; u_h, v_h) = \int_E \frac{\nabla\Pi_E^\nabla u_h \cdot \nabla\Pi_E^\nabla v_h}{f_h^E(w_h)}\, dx + \frac{S^E((I-\Pi_E^\nabla)u_h, (I-\Pi_E^\nabla)v_h)}{f_h^E(w_h)}. \tag{6}$$

Note that as $f_h^E(w_h)$ is constant on each polygon E, the form $A_h^E(\cdot;\cdot,\cdot)$ can be equivalently written as

$$A_h^E(w_h; u_h, v_h) = \frac{a_h^E(u_h, v_h)}{f_h^E(w_h)} \tag{7}$$

where

$$a_h^E(u_h, v_h) = \int_E \nabla\Pi_E^\nabla u_h \cdot \nabla\Pi_E^\nabla v_h dx + S^E((I-\Pi_E^\nabla)u_h, (I-\Pi_E^\nabla)v_h)$$

is the classical local discrete VEM bilinear form for the Laplace problem. It is worth remembering (see, e.g., [10]) that $a_h^E(\cdot,\cdot)$ satisfies the following two crucial properties:

(i) **Consistency**: for every polynomial $q \in \mathbb{P}^1(E)$ and function $v_h \in V_h^E$ we have:

$$a_h^E(v_h, q) = a^E(v_h, q); \tag{8}$$

(ii) **Stability**: there exist two positive constants α_*, α^* independent of h and E such that for every $v_h \in V_h^E$ it holds:

$$\alpha_* a^E(v_h, v_h) \le a_h^E(v_h, v_h) \le \alpha^* a^E(v_h, v_h). \tag{9}$$

Remark that requiring that the stability condition (ii) holds is equivalent to requiring that there exists positive constants $\widetilde{\alpha}_*$ and $\widetilde{\alpha}^*$ such that, for all $v_h \in V_h^E$ with $\Pi_E^\nabla v_h = 0$ it holds:

$$\widetilde{\alpha}_* a^E(v_h, v_h) \le S^E(v_h, v_h) \le \widetilde{\alpha}^* a^E(v_h, v_h), \tag{10}$$

(see [10] for more details). Existence and uniqueness of the solution $u_h \in V_h^\varphi$ follow by working on the discrete cost functional $J_h(v_h)$ as in [13].

For future use, we set $a^E(u_h, v_h) = \int_E \nabla u_h \cdot \nabla v_h dx$.

3 Error analysis

We make the following regularity assumptions on the mesh sequence $\{\mathcal{T}_h\}_h$:

(**H**) there exists a constant $\rho_0 > 0$ independent of $\mathcal{T}_h$, such that for every element E it holds:

(H1) E is star-shaped with respect to all the points of a ball of radius $\rho_0 h_E$

(H2) every edge $e \in \mathcal{E}_h$ has length $|e| \geq \rho_0 h_E$.

The assumptions (H1)-(H2) are standard (see, e.g., [10]) and allow to define, for every smooth enough function v, an "interpolant" v_I in V_h^φ such that it holds $|v - v_I|_{1,\Omega} \lesssim h$ (see [10]).

We now state the main result of the paper.

Theorem 3.1. *Let $u \in H^2(\Omega) \cap W^{1,\infty}(\Omega)$ be the continuous solution to (1), and let $u_h \in V_h^\varphi$ be the VEM solution to (5). Letting*

$$C(u_h) = h^{-1} \sqrt{\sum_E S^E((I - \Pi_E^\nabla)u_h, (I - \Pi_E^\nabla)u_h)},$$

it holds

$$|u - u_h|_{1,\Omega} \lesssim (1 + C(u_h))^2 h. \tag{11}$$

Corollary 3.2. *Assume that $C(u_h) \lesssim 1$. Then it holds that*

$$|u - u_h|_{1,\Omega} \lesssim h.$$

Proof. By triangle inequality we have

$$|u - u_h|_{1,\Omega} \leq |u - u_I|_{1,\Omega} + |u_I - u_h|_{1,\Omega}.$$

In the following, we adapt the ideas of [16] to the present context. We preliminary observe that the following holds true

$$\begin{aligned} |u_I - u_h|_{1,\Omega} &= \left(\sum_{E \in \mathcal{T}_h} \int_E \frac{|\nabla(u_I - u_h)|^2}{f_h^E(u_h)} f_h^E(u_h) \right)^{1/2} \\ &\leq \left(\max_E |f_h^E(u_h)| \right)^{1/2} \left(\sum_{E \in \mathcal{T}_h} \int_E \frac{|\nabla(u_I - u_h)|^2}{f_h^E(u_h)} \right)^{1/2}. \end{aligned} \tag{12}$$

The remaining part of the proof is devoted to show:

(i) $\left(\sum_{E \in \mathcal{T}_h} \int_E \frac{|\nabla(u_I - u_h)|^2}{f_h^E(u_h)} \right)^{1/2} \lesssim (1 + C(u_h))h;$

(ii) $\max_E |f_h^E(u_h)| \lesssim (1 + C(u_h))^2$.

Let us first prove (i). We start by observing that, thanks to (10), we have

$$|u_h - \Pi_E^\nabla u_h|_{1,h} \lesssim C(u_h)h \tag{13}$$

where where $|v|_{1,h}^2 = \sum_{E\in\mathcal{T}_h} \|\nabla v\|_{0,E}^2$. By using the stability property of $a_h^E(\cdot,\cdot)$, as $f_h^E(u_h)$ is constant on E, we get the following inequalities with $\delta_h = u_h - u_I$

$$\begin{aligned}\sum_{E\in\mathcal{T}_h}\int_E \frac{|\nabla(u_I-u_h)|^2}{f_h^E(u_h)} &\lesssim \sum_{E\in\mathcal{T}_h}\frac{a_h^E(\delta_h,\delta_h)}{f_h^E(u_h)} \\ &\lesssim \left|-\sum_{E\in\mathcal{T}_h}\frac{a_h^E(u_I,\delta_h)}{f_h^E(u_h)}\right|, \end{aligned}\tag{14}$$

where in the last step we employ (5) with $\delta_h \in V_h^0$. Let $u_\pi|_E$ be the $L^2(E)$ projection of u onto $\mathbb{P}^1(E)$. By employing the consistency and stability properties of $a_h^E(\cdot,\cdot)$ together with the fact that u is solution to (1), it is immediate to check that the following holds

$$\begin{aligned}-\sum_{E\in\mathcal{T}_h}\frac{a_h^E(u_I,\delta_h)}{f_h^E(u_h)} &= -\sum_{E\in\mathcal{T}_h}\left\{\frac{a_h^E(u_I-u_\pi,\delta_h)}{f_h^E(u_h)} + \frac{a_h^E(u_\pi,\delta_h)}{f_h^E(u_h)}\right. \\ &\quad \left. \pm\frac{a^E(u,\delta_h)}{f_h^E(u_h)} - \int_E \frac{\nabla u\cdot\nabla\delta_h}{f(u)}dx\right\} \qquad (15)\\ &= \sum_{E\in\mathcal{T}_h}\frac{a_h^E(u_\pi-u_I,\delta_h)}{f_h^E(u_h)} + \sum_{E\in\mathcal{T}_h}\frac{a^E(u-u_\pi,\delta_h)}{f_h^E(u_h)} \\ &\quad + \sum_{E\in\mathcal{T}_h}\int_E \nabla u\cdot\nabla\delta_h\left(\frac{1}{f(u)} - \frac{1}{f_h^E(u_h)}\right)dx \\ &= A + B + C. \qquad (16)\end{aligned}$$

We now bound the three terms separately. By combining the Cauchy-Schwarz inequality with the fact that $f_h^E(u_h)$ is constant and larger than 1 on each polygon E, we have

$$A \le (|u-u_\pi|_{1,h} + |u-u_I|_{1,\Omega})\left(\sum_{E\in\mathcal{T}_h}\int_E \frac{|\nabla(u_I-u_h)|^2}{f_h^E(u_h)}dx\right)^{1/2}, \tag{17}$$

and

$$B \le |u-u_\pi|_{1,h}\left(\sum_{E\in\mathcal{T}_h}\int_E \frac{|\nabla(u_I-u_h)|^2}{f_h^E(u_h)}dx\right)^{1/2}. \tag{18}$$

Finally, setting $\gamma = \max_{\bar{\Omega}} \frac{|\nabla u|}{f(u)}$, employing the definitions of $f(\cdot)$ and $f_h^E(\cdot)$ and observing that $f(u) \geq |\nabla u|$, the following holds

$$\begin{aligned} C &= \sum_{E\in\mathcal{T}_h} \int_E \nabla u \cdot \nabla \delta_h \frac{[f_h^E(u_h)]^2 - f^2(u)}{f(u) f_h^E(u_h)(f(u) + f_h^E(u_h))} dx \\ &\leq \gamma \sum_{E\in\mathcal{T}_h} \int_E |\nabla \delta_h| \frac{|f^2(u) - [f_h^E(u_h)]^2|}{f_h^E(u_h)(f(u) + f_h^E(u_h))} dx \\ &= \gamma \sum_{E\in\mathcal{T}_h} \left\{ \int_E |\nabla \delta_h| \frac{\big||\nabla u|^2 - |\nabla \Pi_E^\nabla u_h|^2\big|}{f_h^E(u_h)(f(u) + f_h^E(u_h))} dx \right. \\ &\quad \left. + \int_E |\nabla \delta_h| \frac{|E|^{-1} S^E((I - \Pi_E^\nabla)u_h, (I - \Pi_E^\nabla)u_h))}{f_h^E(u_h)(f(u) + f_h^E(u_h))} dx \right\} = C.I + C.II \end{aligned}$$

As $f_h^E(u_h) \geq |\nabla \Pi_E^\nabla u_h|$, we can bound

$$\begin{aligned} C.I &= \gamma \sum_{E\in\mathcal{T}_h} \int_E |\nabla \delta_h| \frac{\big||\nabla u|^2 - |\nabla \Pi_E^\nabla u_h|^2\big|}{f_h^E(u_h)(f(u) + f_h^E(u_h))} dx \\ &\leq \gamma \sum_{E\in\mathcal{T}_h} \int_E |\nabla \delta_h| \frac{|\nabla(u - \Pi_E^\nabla u_h)|(|\nabla u| + |\nabla \Pi_E^\nabla u_h|)}{f_h^E(u_h)(f(u) + f_h^E(u_h))} dx \\ &\leq \gamma \sum_{E\in\mathcal{T}_h} \int_E |\nabla \delta_h| \frac{|\nabla(u - \Pi_E^\nabla u_h)|}{f_h^E(u_h)} dx. \end{aligned}$$

Now, employing the Cauchy-Schwarz inequality and noticing that $f_h^E(u_h) \geq 1$, we have the following

$$\begin{aligned} C.I &\lesssim \gamma \left(\sum_{E\in\mathcal{T}_h} \int_E \frac{|\nabla \delta_h|^2}{f_h^E(u_h)} dx \right)^{1/2} \left\{ \left(\sum_{E\in\mathcal{T}_h} \int_E \frac{|\nabla \delta_h|^2}{f_h^E(u_h)} dx \right)^{1/2} + |u - u_I|_{1,\Omega} + |u_h - \Pi_E^\nabla u_h|_{1,h} \right\} \\ &\leq \gamma \left(\sum_{E\in\mathcal{T}_h} \int_E \frac{|\nabla \delta_h|^2}{f_h^E(u_h)} dx \right)^{1/2} \left\{ \left(\sum_{E\in\mathcal{T}_h} \int_E \frac{|\nabla \delta_h|^2}{f_h^E(u_h)} dx \right)^{1/2} + |u - u_I|_{1,\Omega} + C(u_h)h \right\}, \end{aligned} \tag{19}$$

where we used the stability property (13) and the definition of the constant $C(u_h)$. On the other hand, as $f_h^E(u_h) > 1$ clearly implies $[f_h^E(u_h)]^2 \geq [f_h^E(u_h)]^{3/2}$, we have

$$\begin{aligned} C.II &\leq \gamma \sum_{E\in\mathcal{T}_h} \int_E \frac{|\nabla \delta_h|}{2[f_h^E(u_h)]^{1/2}} \frac{|E|^{-1} S^E((I - \Pi_E^\nabla)u_h, (I - \Pi_E^\nabla)u_h))}{f_h^E(u_h)} dx \\ &\leq \gamma \sum_{E\in\mathcal{T}_h} \int_E \frac{|\nabla \delta_h|}{2[f_h^E(u_h)]^{1/2}} |E|^{-1/2} (S^E((I - \Pi_E^\nabla)u_h, (I - \Pi_E^\nabla)u_h)))^{1/2} dx \\ &\leq \gamma \left(\sum_{E\in\mathcal{T}_h} \int_E \frac{|\nabla \delta_h|^2}{f_h^E(u_h)} dx \right)^{1/2} C(u_h)h, \end{aligned} \tag{20}$$

where we used $f_h^E(u_h) \geq |E|^{-1/2}(S^E((I-\Pi_E^\nabla)u_h,(I-\Pi_E^\nabla)u_h)))^{1/2}$ and employed the Cauchy-Schwarz inequality once again. Setting

$$T = \sum_{E\in\mathcal{T}_h} \int_E \frac{|\nabla\delta_h|^2}{f_h^E(u_h)}dx$$

and plugging the above inequalities for A, B, C into (14) we obtain

$$T \lesssim T^{\frac{1}{2}}(|u-u_\pi|_{1,h} + |u-u_I|_{1,\Omega}) + T^{\frac{1}{2}}|u-u_\pi|_{1,h} \\ + \gamma T^{\frac{1}{2}}\left(T^{\frac{1}{2}} + |u-u_I|_{1,\Omega} + 2C(u_h)h\right).$$

Noticing that $\gamma < 1$ we get

$$T^{1/2} \lesssim \frac{1}{1-\gamma}(|u-u_\pi|_{1,h} + |u-u_I|_1 + C(u_h)h), \tag{21}$$

which, using standard error estimates, implies $T^{1/2} \lesssim (1+C(u_h))h$.

Finally, we prove (ii). In particular, from (i) we have

$$\left(\int_E \frac{|\nabla\delta_h|^2}{f_h^E(u_h)}dx\right)^{1/2} \lesssim (1+C(u_h))h$$

for any $E \in \mathcal{T}_h$, which implies

$$\begin{aligned}\left(\int_E \frac{|\nabla u_h|^2}{f_h^E(u_h)}dx\right)^{1/2} &\lesssim \left(\int_E \frac{|\nabla\delta_h|^2}{f_h^E(u_h)}dx\right)^{1/2} + \left(\int_E \frac{|\nabla u_I|^2}{f_h^E(u_h)}dx\right)^{1/2} \\ &\lesssim (1+C(u_h))h + |u|_{W^{1,\infty}}\left(\int_E dx\right)^{1/2} \\ &\lesssim (1+C(u_h))h, \end{aligned} \tag{22}$$

where we employed the fact that $f_h^E(u_h) \geq 1$ on each E, the H^1-stability of the interpolation operator $(\cdot)_I$ and $|E| \simeq h^2$.

On the other hand, using the fact that $f_h^E(u_h)$ is constant on each E and employing the H^1-orthogonality property of the elliptic projector Π_E^∇ we have

$$\begin{aligned}\int_E \frac{|\nabla u_h|^2}{f_h^E(u_h)}dx &= \int_E \frac{|\nabla\Pi_E^\nabla u_h|^2}{f_h^E(u_h)}dx + \int_E \frac{|\nabla(I-\Pi_E^\nabla)u_h|^2}{f_h^E(u_h)}dx \\ &\geq \int_E \frac{|\nabla\Pi_E^\nabla u_h|^2}{f_h^E(u_h)}dx + \frac{S^E((I-\Pi_E^\nabla)u_h,(I-\Pi_E^\nabla)u_h)}{f_h^E(u_h)}, \end{aligned} \tag{23}$$

where in the last step we employed (10). Combining (22) and (23), and observing that $\Pi_E^\nabla u_h$ and $S^E((I-\Pi_E^\nabla)u_h,(I-\Pi_E^\nabla)u_h)$ are both constant on E yield

$$\int_E \frac{|\nabla\Pi_E^\nabla u_h|^2 + |E|^{-1}S^E((I-\Pi_E^\nabla)u_h,(I-\Pi_E^\nabla)u_h)}{f_h^E(u_h)}dx \lesssim (1+C(u_h))^2h^2,$$

and thus

$$\frac{|\nabla \Pi_E^\nabla u_h|^2 + |E|^{-1} S^E((I - \Pi_E^\nabla)u_h, (I - \Pi_E^\nabla)u_h)}{f_h^E(u_h)} \lesssim (1 + C(u_h))^2,$$

which, recalling the definition of $f_h^E(u_h)$, implies

$$|\nabla \Pi_E^\nabla u_h|^2 + |E|^{-1} S^E((I - \Pi_E^\nabla)u_h, (I - \Pi_E^\nabla)u_h) \lesssim (1 + C(u_h))^4.$$

This yields (ii). By combining (i) and (ii) with (12) we finally obtain the thesis. □

Remark 3.3. Observe that, while (11) is not properly an *a priori* estimate on the error, as the quantity $C(u_h)$ on the right hand side depends on the discrete solution and, consequently on h, such a quantity can be computed *a posteriori*, allowing us to check whether it remains bounded, thus providing a useful bound. Observe also that such a quantity is obtained by combining local contributions, so that, should it be too big, its distribution might (heuristically) provide some information on how to refine the mesh in order to obtain a better solution.

4 Numerical Experiments

The discrete VE problem (5) is solved using a classical fixed point algorithm, i.e. iterate on k the following: given $u_h^k \in V_h^\varphi$, find $u_h^{k+1} \in V_h^\varphi$ such that

$$A_h(u_h^k; u_h^{k+1}, v_h) = 0 \qquad \forall\, v_h \in V_h^0 \quad (\textit{linearized problem}).$$

Fixed point iterations are stopped as soon as $||u_h^{k+1} - u_h^k||_\infty / ||u_h^k||_\infty$ is less than a prescribed tolerance $\texttt{tol} = 10^{-9}$, whereas at each iteration, the discrete linear system is solved using a direct solver.

To assess the convergence properties of our Virtual Element discretization, we introduce the following error quantities:

$$e_{H^1} = \frac{||\nabla u - \Pi_0^0 \nabla u_h||_{L^2(\Omega)}}{||\nabla u||_{L^2(\Omega)}}, \qquad e_{L^2} = \frac{||u - \Pi_1^0 u_h||_{L^2(\Omega)}}{||u||_{L^2(\Omega)}},$$

where Π_k^0 is the L^2-projection onto the space of polynomials of degree k, $k = 0, 1$. The exact solution u is evaluated analytically, whenever possible. Otherwise, it is approximated by the solution u_h^{FEM} computed with the finite element method on a very fine grid of Ω. Estimated convergence rates (ecr) are computed with respect to the total number of degrees of freedom N, under the assumption $N \approx O(h^{-2})$. All the numerical experiments are performed on Voronoi meshes that are either uniform or random, see Figure 1. For each mesh, we collect the following informations (see tables below):

- the maximum diameter over all the elements of the mesh (h);
- the number of degrees of freedom (N);

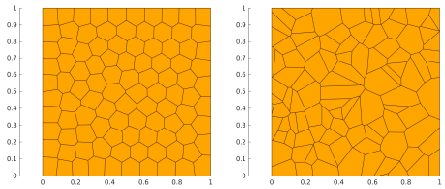

Figure 1: Example of the meshes used in the numerical tests.

- the number of fixed-point iterations required to reach convergence (It);
- the computed errors e_{H^1} and e_{L^2} measured in the H^1 and L^2 norms, respectively, and the corresponding estimated convergence rates (ecr);
- the constant $C(u_h)$ defined in Theorem 3.1, computed by using either the actual diameter h (see the column named C_1) or $1/\sqrt{N} \approx h$ (see the column named C_2).

4.1 Test 1

Here we consider a test problem originally proposed by Concus [14] that provided the following analytic solution to the minimal surface problem on the square $\Omega = (0.25, 0.75) \times (0.25, 0.75)$:

$$u(x, y) = \sqrt{\cosh^2(y) - x^2}.$$

Note that $u \in H^2(\Omega) \cap W^{1,\infty}(\Omega)$. An example of computed solution on a coarse mesh is shown in Figure 2. Experiments are performed on uniform (Table 1) and random Voronoi meshes (Table 2). The assumption $C(u_h) \lesssim 1$ is verified and the rate of convergence in the H^1-norm is in agreement with Theorem 3.1. Moreover, the reported rate of convergence in the L^2-norm seems to be 2.

4.2 Test 2

Here we consider another test problem for which an analytic solution is known [18]. Let us consider the following convex domain

$$\Omega = \left\{ \mathbf{x} = (x, y) \in \mathbb{R}^2 \;\middle|\; \|\mathbf{x}\|_2 < 4 \cap x > 1 \right\}.$$

An explicit example of minimal surface on Ω is given by

$$u(x, y) = a \log \left(\frac{b + \sqrt{b^2 - a^2}}{r + \sqrt{r^2 - a^2}} \right),$$

where we take $a = 0.75, b = 4$ and $r = \sqrt{x^2 + y^2}$. Note that $u \in H^2(\Omega) \cap W^{1,\infty}(\Omega)$. This minimal surface is also known as *catenoid*. A typical solution

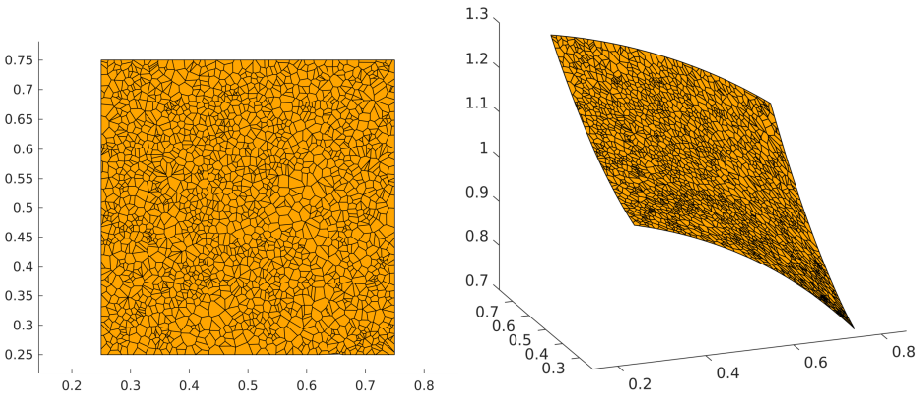

Figure 2: Example 4.1: example of the computational mesh (left) and corresponding computed solution (right).

Table 1: Example 4.1: computed errors and estimated convergence rates (uniform Voronoi meshes).

Mesh	h	N	It	e_{H^1}	ecr	e_{L^2}	ecr	C_1	C_2
u-concus$_1$	$1.82{\cdot}10^{-2}$	4082	17	$7.32{\cdot}10^{-3}$	-	$1.23{\cdot}10^{-5}$	-	0.13	0.16
u-concus$_2$	$1.23{\cdot}10^{-2}$	8165	17	$5.14{\cdot}10^{-3}$	1.02	$6.18{\cdot}10^{-6}$	1.98	0.14	0.15
u-concus$_3$	$8.47{\cdot}10^{-3}$	16 323	17	$3.64{\cdot}10^{-3}$	0.99	$3.21{\cdot}10^{-6}$	1.89	0.15	0.16
u-concus$_4$	$6.36{\cdot}10^{-3}$	32 657	17	$2.56{\cdot}10^{-3}$	1.01	$1.52{\cdot}10^{-6}$	2.15	0.14	0.16
u-concus$_5$	$4.51{\cdot}10^{-3}$	65 293	17	$1.82{\cdot}10^{-3}$	0.99	$7.96{\cdot}10^{-7}$	1.87	0.14	0.16
u-concus$_6$	$3.00{\cdot}10^{-3}$	130 567	17	$1.28{\cdot}10^{-3}$	1.00	$4.04{\cdot}10^{-7}$	1.96	0.15	0.16
u-concus$_7$	$2.24{\cdot}10^{-3}$	261 206	17	$9.08{\cdot}10^{-4}$	1.00	$1.98{\cdot}10^{-7}$	2.06	0.14	0.16
u-concus$_8$	$1.52{\cdot}10^{-3}$	522 279	17	$6.42{\cdot}10^{-4}$	1.00	$9.94{\cdot}10^{-8}$	1.99	0.14	0.16

Table 2: Example 4.1: computed errors and estimated convergence rates (random Voronoi meshes).

Mesh	h	N	It	e_{H^1}	ecr	e_{L^2}	ecr	C_1	C_2
concus$_1$	$3.41{\cdot}10^{-2}$	3716	17	$9.32{\cdot}10^{-3}$	-	$2.74{\cdot}10^{-5}$	-	0.09	0.19
concus$_2$	$2.53{\cdot}10^{-2}$	7450	17	$6.41{\cdot}10^{-3}$	1.08	$1.11{\cdot}10^{-5}$	2.58	0.08	0.18
concus$_3$	$1.72{\cdot}10^{-2}$	14 693	17	$4.58{\cdot}10^{-3}$	0.99	$5.94{\cdot}10^{-6}$	1.85	0.09	0.19
concus$_4$	$1.29{\cdot}10^{-2}$	29 487	17	$3.22{\cdot}10^{-3}$	1.01	$3.04{\cdot}10^{-6}$	1.92	0.08	0.19
concus$_5$	$9.16{\cdot}10^{-3}$	59 011	17	$2.26{\cdot}10^{-3}$	1.02	$1.58{\cdot}10^{-6}$	1.89	0.08	0.18
concus$_6$	$7.24{\cdot}10^{-3}$	118 053	17	$1.60{\cdot}10^{-3}$	1.00	$7.45{\cdot}10^{-7}$	2.17	0.07	0.19
concus$_7$	$4.92{\cdot}10^{-3}$	235 898	17	$1.13{\cdot}10^{-3}$	1.00	$3.71{\cdot}10^{-7}$	2.02	0.08	0.19
concus$_8$	$3.57{\cdot}10^{-3}$	472 263	17	$8.01{\cdot}10^{-4}$	1.00	$1.84{\cdot}10^{-7}$	2.02	0.08	0.19

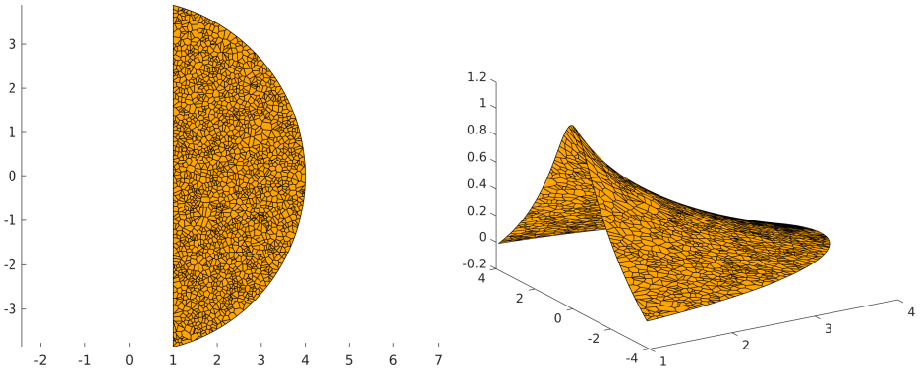

Figure 3: Example 4.2: example of the computational mesh (left) and corresponding computed solution (right).

Table 3: Example 4.2: computed errors and estimated convergence rates (uniform Voronoi meshes).

Mesh	h	N	It	e_{H^1}	ecr	e_{L^2}	ecr	C_1	C_2
u-sector$_1$	$1.41{\cdot}10^{-1}$	4080	20	$2.57{\cdot}10^{-2}$	-	$3.75{\cdot}10^{-4}$	-	0.20	1.78
u-sector$_2$	$1.03{\cdot}10^{-1}$	8158	21	$1.75{\cdot}10^{-2}$	1.11	$1.72{\cdot}10^{-4}$	2.25	0.19	1.74
u-sector$_3$	$6.98{\cdot}10^{-2}$	16 309	21	$1.26{\cdot}10^{-2}$	0.94	$8.94{\cdot}10^{-5}$	1.89	0.20	1.77
u-sector$_4$	$5.18{\cdot}10^{-2}$	32 640	22	$8.94{\cdot}10^{-3}$	1.00	$4.51{\cdot}10^{-5}$	1.97	0.19	1.76
u-sector$_5$	$3.59{\cdot}10^{-2}$	65 271	22	$6.38{\cdot}10^{-3}$	0.97	$2.29{\cdot}10^{-5}$	1.96	0.19	1.78
u-sector$_6$	$2.56{\cdot}10^{-2}$	130 572	23	$4.43{\cdot}10^{-3}$	1.05	$1.12{\cdot}10^{-5}$	2.08	0.19	1.74
u-sector$_7$	$1.81{\cdot}10^{-2}$	261 077	23	$3.14{\cdot}10^{-3}$	0.99	$5.58{\cdot}10^{-6}$	2.00	0.19	1.76
u-sector$_8$	$1.30{\cdot}10^{-2}$	522 210	23	$2.22{\cdot}10^{-3}$	1.01	$2.76{\cdot}10^{-6}$	2.03	0.19	1.76

on a coarse mesh is shown in Figure 3. Experiments are performed on uniform Voronoi meshes (Table 3) and random Voronoi meshes (Table 4). Again, $C(u_h) \lesssim 1$ and the rate of convergence in the H^1-norm is in agreement with Theorem 3.1, whereas the computed rate of convergence in the L^2-norm seems to be 2.

4.3 Test 3

Here we consider the so called Scherk's fifth surface [19] which is another minimal surface that can be expressed on $\Omega = (-0.8, 0.8) \times (-0.8, 0.8)$ as follows

$$u(x, y) = \sin^{-1}(\sinh x \sinh y).$$

A typical solution on a coarse mesh is shown in Figure 4. Experiments are performed on uniform Voronoi meshes (Table 5) and random Voronoi meshes (Table 6). The assumption $C(u_h) \lesssim 1$ is satisfied, and, as predicted by our

Table 4: Example 4.2: computed errors and estimated convergence rates (random Voronoi meshes).

Mesh	h	N	It	e_{H^1}	ecr	e_{L^2}	ecr	C_1	C_2
sector_1	$2.78{\cdot}10^{-1}$	4198	19	$3.04{\cdot}10^{-2}$	-	$6.54{\cdot}10^{-4}$	-	0.12	2.18
sector_2	$2.26{\cdot}10^{-1}$	8330	19	$2.30{\cdot}10^{-2}$	0.81	$3.99{\cdot}10^{-4}$	1.44	0.11	2.27
sector_3	$1.48{\cdot}10^{-1}$	16 588	21	$1.54{\cdot}10^{-2}$	1.18	$1.61{\cdot}10^{-4}$	2.64	0.11	2.18
sector_4	$1.07{\cdot}10^{-1}$	33 080	22	$1.11{\cdot}10^{-2}$	0.95	$8.75{\cdot}10^{-5}$	1.76	0.11	2.22
sector_5	$7.99{\cdot}10^{-2}$	65 973	22	$7.81{\cdot}10^{-3}$	1.01	$4.46{\cdot}10^{-5}$	1.95	0.11	2.23
sector_6	$5.48{\cdot}10^{-2}$	131 673	23	$5.48{\cdot}10^{-3}$	1.03	$2.08{\cdot}10^{-5}$	2.21	0.11	2.21
sector_7	$4.04{\cdot}10^{-2}$	262 975	23	$3.90{\cdot}10^{-3}$	0.98	$1.06{\cdot}10^{-5}$	1.96	0.11	2.25
sector_8	$2.85{\cdot}10^{-2}$	525 468	23	$2.72{\cdot}10^{-3}$	1.03	$5.12{\cdot}10^{-6}$	2.09	0.11	2.23

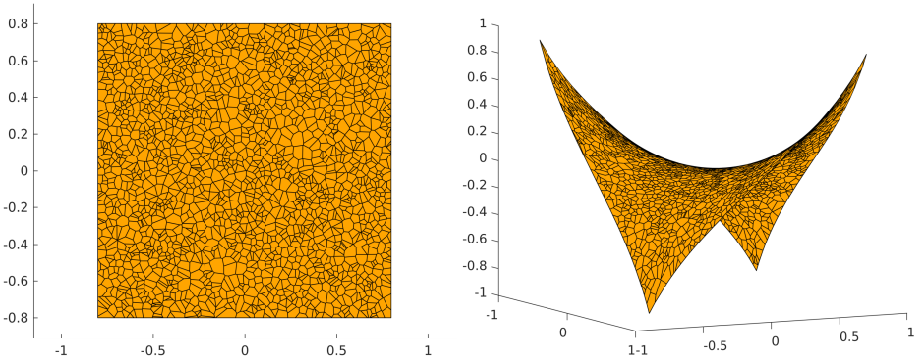

Figure 4: Example 4.3: example of the computational mesh (left) and corresponding computed solution (right).

theoretical analysis, we observe a linear convergence in the H^1 norm. Moreover, second order convergence in the L^2 norm is also observed.

4.4 Test 4

The minimal surface problem (4) is solved on $\Omega = (0,1)^2$ with the following boundary conditions

$$\begin{cases} \varphi = 0 & \text{on } y = 0 \text{ and } x = 0, \\ \varphi = x & \text{on } y = 1, \\ \varphi = y & \text{on } x = 1. \end{cases}$$

A typical solution on a coarse mesh is shown in Figure 5. We recall that by properly rotating and translating this minimal surface, it is possible to obtain the so-called Schwarz D surface (see Figure 6). Results on uniform and random Voronoi meshes are shown in Tables 7 and 8, respectively. The reference FEM

Table 5: Example 4.3: computed errors and estimated convergence rates (uniform Voronoi meshes).

Mesh	h	N	It	e_{H^1}	ecr	e_{L^2}	ecr	C_1	C_2
u-scherk$_1$	$5.85{\cdot}10^{-2}$	4079	25	$2.83{\cdot}10^{-2}$	-	$7.51{\cdot}10^{-4}$	-	0.55	2.05
u-scherk$_2$	$3.88{\cdot}10^{-2}$	8158	27	$1.97{\cdot}10^{-2}$	1.04	$3.57{\cdot}10^{-4}$	2.14	0.56	1.97
u-scherk$_3$	$2.79{\cdot}10^{-2}$	16 323	29	$1.40{\cdot}10^{-2}$	0.99	$1.80{\cdot}10^{-4}$	1.97	0.55	1.96
u-scherk$_4$	$1.96{\cdot}10^{-2}$	32 664	31	$9.79{\cdot}10^{-3}$	1.03	$8.67{\cdot}10^{-5}$	2.11	0.54	1.92
u-scherk$_5$	$1.38{\cdot}10^{-2}$	65 275	29	$6.99{\cdot}10^{-3}$	0.97	$4.50{\cdot}10^{-5}$	1.89	0.54	1.91
u-scherk$_6$	$1.01{\cdot}10^{-2}$	130 555	30	$4.92{\cdot}10^{-3}$	1.01	$2.27{\cdot}10^{-5}$	1.98	0.52	1.89
u-scherk$_7$	$7.06{\cdot}10^{-3}$	261 164	31	$3.48{\cdot}10^{-3}$	1.00	$1.12{\cdot}10^{-5}$	2.02	0.52	1.89
u-scherk$_8$	$5.04{\cdot}10^{-3}$	522 210	30	$2.47{\cdot}10^{-3}$	0.99	$5.61{\cdot}10^{-6}$	2.00	0.52	1.88

Table 6: Example 4.3: computed errors and estimated convergence rates (random Voronoi meshes).

Mesh	h	N	It	e_{H^1}	ecr	e_{L^2}	ecr	C_1	C_2
scherk$_1$	$1.18{\cdot}10^{-1}$	4098	29	$3.54{\cdot}10^{-2}$	-	$1.45{\cdot}10^{-3}$	-	0.31	2.36
scherk$_2$	$7.67{\cdot}10^{-2}$	8197	31	$2.44{\cdot}10^{-2}$	1.07	$6.57{\cdot}10^{-4}$	2.28	0.33	2.32
scherk$_3$	$5.48{\cdot}10^{-2}$	16 391	34	$1.76{\cdot}10^{-2}$	0.95	$3.76{\cdot}10^{-4}$	1.61	0.33	2.30
scherk$_4$	$4.15{\cdot}10^{-2}$	32 778	34	$1.25{\cdot}10^{-2}$	0.98	$1.73{\cdot}10^{-4}$	2.24	0.31	2.33
scherk$_5$	$2.85{\cdot}10^{-2}$	65 551	33	$8.77{\cdot}10^{-3}$	1.03	$8.59{\cdot}10^{-5}$	2.02	0.32	2.31
scherk$_6$	$2.13{\cdot}10^{-2}$	131 087	36	$6.22{\cdot}10^{-3}$	0.99	$4.45{\cdot}10^{-5}$	1.90	0.30	2.31
scherk$_7$	$1.75{\cdot}10^{-2}$	262 167	35	$4.35{\cdot}10^{-3}$	1.03	$2.10{\cdot}10^{-5}$	2.17	0.26	2.29
scherk$_8$	$1.08{\cdot}10^{-2}$	524 326	32	$3.10{\cdot}10^{-3}$	0.98	$1.08{\cdot}10^{-5}$	1.93	0.29	2.30

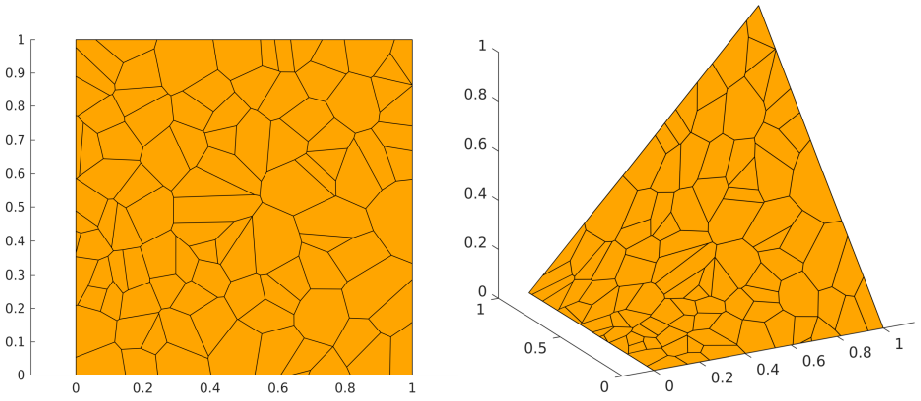

Figure 5: Example 4.4: example of the computational mesh (left) and corresponding computed solution (right).

Table 7: Example 4.4: computed errors and estimated convergence rates (uniform Voronoi meshes).

Mesh	h	N	It	e_{H^1}	ecr	e_{L^2}	ecr	C_1	C_2
u-square$_1$	$3.40{\cdot}10^{-2}$	4077	22	$1.14{\cdot}10^{-2}$	-	$1.12{\cdot}10^{-4}$	-	0.23	0.50
u-square$_2$	$2.70{\cdot}10^{-2}$	8155	22	$8.00{\cdot}10^{-3}$	1.02	$5.50{\cdot}10^{-5}$	2.05	0.20	0.49
u-square$_3$	$1.74{\cdot}10^{-2}$	16 325	22	$5.70{\cdot}10^{-3}$	0.98	$2.78{\cdot}10^{-5}$	1.97	0.22	0.49
u-square$_4$	$1.21{\cdot}10^{-2}$	32 636	22	$4.02{\cdot}10^{-3}$	1.00	$1.39{\cdot}10^{-5}$	2.01	0.23	0.49
u-square$_5$	$8.70{\cdot}10^{-3}$	65 297	22	$2.85{\cdot}10^{-3}$	1.00	$6.89{\cdot}10^{-6}$	2.02	0.22	0.49
u-square$_6$	$6.11{\cdot}10^{-3}$	130 532	22	$2.02{\cdot}10^{-3}$	0.99	$3.44{\cdot}10^{-6}$	2.00	0.22	0.49
u-square$_7$	$4.47{\cdot}10^{-3}$	261 135	22	$1.44{\cdot}10^{-3}$	0.98	$1.72{\cdot}10^{-6}$	2.00	0.21	0.49
u-square$_8$	$3.11{\cdot}10^{-3}$	522 236	22	$1.03{\cdot}10^{-3}$	0.97	$8.60{\cdot}10^{-7}$	2.00	0.22	0.49

solution is computed on a Delaunay triangular mesh with 7767583 nodes and 15524627 triangles. Also in this case we observe $C(u_h) \lesssim 1$, a linear convergence in the H^1 norm, and a quadratic convergence in the L^2 norm.

4.5 Test 5

Here we consider a minimal surface problem on the unit disk, where the boundary condition is $\varphi(x, y) = x^2$. A typical solution on a coarse mesh is shown in Figure 7. Results on uniform and random Voronoi meshes are shown in Tables 9 and 10, respectively. Again, $C(u_h) \lesssim 1$ and we observe a linear convergence in the H^1 norm. Moreover, second order convergence in the L^2 norm is also observed.

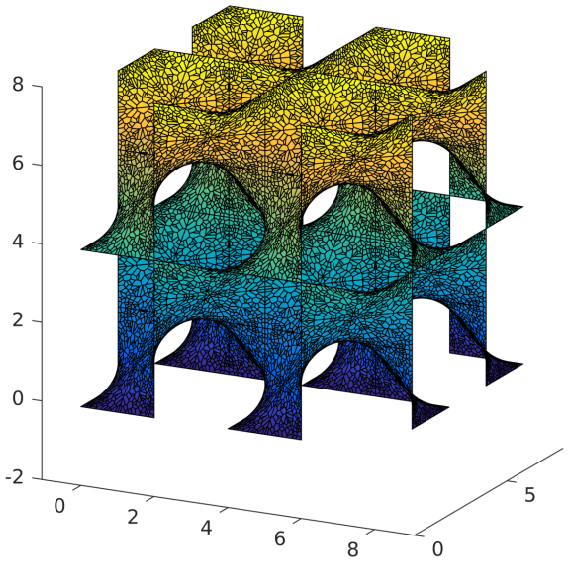

Figure 6: Example 4.4: representation of the Schwarz D surface obtained by rotating and translating the *patch* shown in Figure 5.

Table 8: Example 4.4: computed errors and estimated convergence rates (random Voronoi meshes).

Mesh	h	N	It	e_{H^1}	ecr	e_{L^2}	ecr	C_1	C_2
square_1	$6.38{\cdot}10^{-2}$	5006	22	$1.28{\cdot}10^{-2}$	-	$1.71{\cdot}10^{-4}$	-	0.14	0.61
square_2	$4.34{\cdot}10^{-2}$	10 008	22	$9.09{\cdot}10^{-3}$	0.99	$8.51{\cdot}10^{-5}$	2.02	0.14	0.62
square_3	$3.47{\cdot}10^{-2}$	20 007	22	$6.38{\cdot}10^{-3}$	1.02	$4.19{\cdot}10^{-5}$	2.05	0.13	0.62
square_4	$2.41{\cdot}10^{-2}$	40 011	22	$4.51{\cdot}10^{-3}$	1.00	$2.08{\cdot}10^{-5}$	2.02	0.13	0.61
square_5	$1.73{\cdot}10^{-2}$	80 007	22	$3.21{\cdot}10^{-3}$	0.98	$1.06{\cdot}10^{-5}$	1.95	0.13	0.62
square_6	$1.14{\cdot}10^{-2}$	160 028	22	$2.27{\cdot}10^{-3}$	1.00	$5.25{\cdot}10^{-6}$	2.03	0.14	0.62
square_7	$8.86{\cdot}10^{-3}$	320 020	22	$1.61{\cdot}10^{-3}$	0.98	$2.63{\cdot}10^{-6}$	1.99	0.12	0.62
square_8	$6.25{\cdot}10^{-3}$	640 035	22	$1.15{\cdot}10^{-3}$	0.98	$1.31{\cdot}10^{-6}$	2.01	0.12	0.62

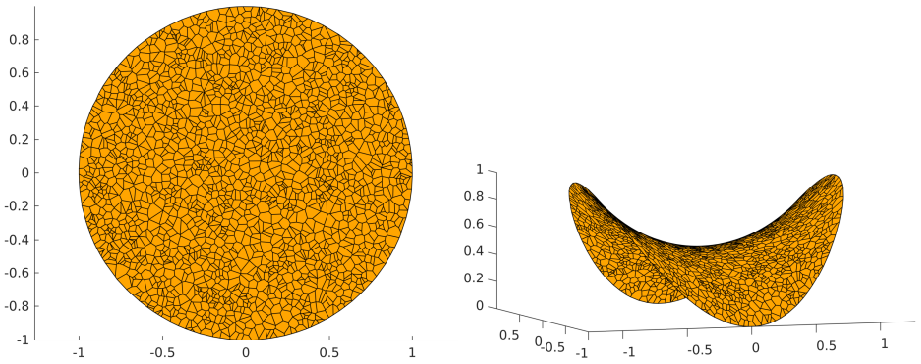

Figure 7: Example 4.5: example of the computational mesh (left) and corresponding computed solution (right).

Table 9: Example 4.5: computed errors and estimated convergence rates (uniform Voronoi meshes).

Mesh	h	N	It	e_{H^1}	ecr	e_{L^2}	ecr	C_1	C_2
u-circ$_1$	$6.17{\cdot}10^{-2}$	4074	22	$2.49{\cdot}10^{-2}$	-	$2.18{\cdot}10^{-4}$	-	0.42	1.64
u-circ$_2$	$4.25{\cdot}10^{-2}$	8166	22	$1.76{\cdot}10^{-2}$	1.00	$1.09{\cdot}10^{-4}$	2.00	0.43	1.64
u-circ$_3$	$3.05{\cdot}10^{-2}$	16 303	22	$1.24{\cdot}10^{-2}$	1.00	$5.40{\cdot}10^{-5}$	2.03	0.42	1.65
u-circ$_4$	$2.16{\cdot}10^{-2}$	32 619	22	$8.80{\cdot}10^{-3}$	1.00	$2.69{\cdot}10^{-5}$	2.01	0.42	1.63
u-circ$_5$	$1.51{\cdot}10^{-2}$	65 275	23	$6.23{\cdot}10^{-3}$	0.99	$1.35{\cdot}10^{-5}$	1.99	0.43	1.64
u-circ$_6$	$1.06{\cdot}10^{-2}$	130 546	23	$4.43{\cdot}10^{-3}$	0.99	$6.72{\cdot}10^{-6}$	2.01	0.43	1.64
u-circ$_7$	$7.73{\cdot}10^{-3}$	261 069	23	$3.16{\cdot}10^{-3}$	0.97	$3.35{\cdot}10^{-6}$	2.00	0.41	1.64
u-circ$_8$	$5.46{\cdot}10^{-3}$	522 188	23	$2.27{\cdot}10^{-3}$	0.95	$1.68{\cdot}10^{-6}$	2.00	0.41	1.64

Table 10: Example 4.5: computed errors and estimated convergence rates (random Voronoi meshes).

Mesh	h	N	It	e_{H^1}	ecr	e_{L^2}	ecr	C_1	C_2
circ$_1$	$1.21{\cdot}10^{-1}$	4238	21	$3.11{\cdot}10^{-2}$	-	$4.28{\cdot}10^{-4}$	-	0.27	2.13
circ$_2$	$8.72{\cdot}10^{-2}$	8398	22	$2.19{\cdot}10^{-2}$	1.03	$2.05{\cdot}10^{-4}$	2.15	0.26	2.11
circ$_3$	$6.23{\cdot}10^{-2}$	16 662	22	$1.55{\cdot}10^{-2}$	1.01	$1.02{\cdot}10^{-4}$	2.03	0.26	2.10
circ$_4$	$4.55{\cdot}10^{-2}$	33 175	22	$1.09{\cdot}10^{-2}$	1.00	$5.07{\cdot}10^{-5}$	2.04	0.25	2.10
circ$_5$	$3.38{\cdot}10^{-2}$	66 096	23	$7.74{\cdot}10^{-3}$	1.00	$2.54{\cdot}10^{-5}$	2.00	0.24	2.08
circ$_6$	$2.42{\cdot}10^{-2}$	131 883	23	$5.48{\cdot}10^{-3}$	1.00	$1.26{\cdot}10^{-5}$	2.03	0.24	2.08
circ$_7$	$1.80{\cdot}10^{-2}$	263 268	23	$3.90{\cdot}10^{-3}$	0.98	$6.31{\cdot}10^{-6}$	2.01	0.22	2.08
circ$_8$	$1.20{\cdot}10^{-2}$	525 901	23	$2.78{\cdot}10^{-3}$	0.97	$3.12{\cdot}10^{-6}$	2.03	0.24	2.08

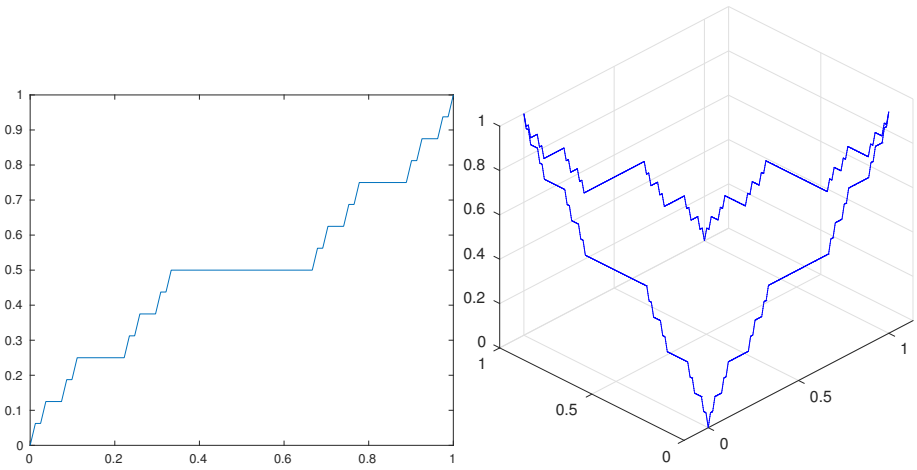

Figure 8: Example 4.6: fourth iterate of a sequence of function converging to the Cantor function on $[0, 1]$ (left) which is used as as boundary condition for Example 4.6 (right).

4.6 Test 6

In the last example, the minimal surface problem is again solved on $\Omega = (0, 1)^2$. As Dirichlet boundary conditions, we require the solution to match proper reflections of the fourth iterate of a sequence of functions converging to the Cantor function (see Figure 8). Note that the exact solution does not satisfy the regularity assumptions of Theorem 3.1. A typical solution on a coarse mesh is shown in Figure 9. Results on uniform and random Voronoi meshes are shown in Tables 11 and 12, respectively. The reference FEM solution is computed on a Delaunay triangular mesh with 7768041 nodes and 15525051 triangles. Such mesh is constructed in order to have all the nodes where the Dirichlet data is just continuous as boundary nodes. Observe that the assumption $C(u_h) \lesssim 1$ does not hold in this case. This example shows that a lack of regularity in the boundary data may severely affect the convergence properties of the method.

5 Conclusions

We presented the lowest order Virtual Element discretization of a minimal surface problem. Optimal error estimate in the H^1-norm has been derived and several numerical tests assessing the validity of the theoretical results have been presented. Moreover, the convergence properties in the L^2-norm has been numerically investigated.

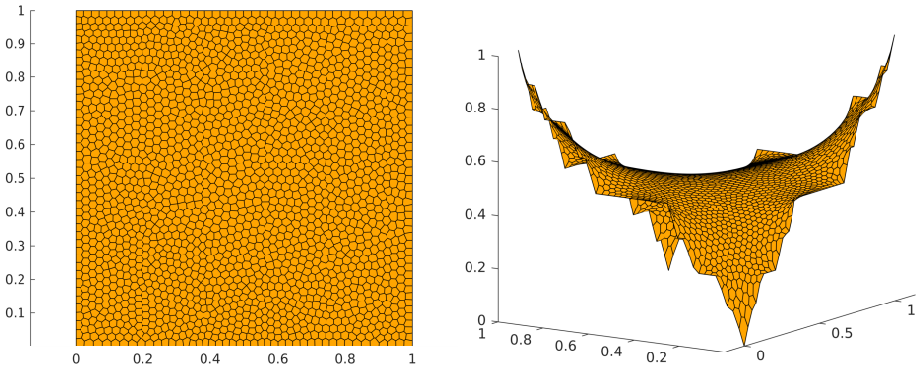

Figure 9: Example 4.6: example of the computational mesh (left) and corresponding computed solution (right).

Table 11: Example 4.6: computed errors and estimated convergence rates (uniform Voronoi meshes).

Mesh	h	N	It	e_{H^1}	ecr	e_{L^2}	ecr	C_1	C_2
u-square$_1$	$3.40{\cdot}10^{-2}$	4077	31	$4.61{\cdot}10^{-1}$	-	$3.01{\cdot}10^{-2}$	-	3.37	7.33
u-square$_2$	$2.70{\cdot}10^{-2}$	8155	45	$4.19{\cdot}10^{-1}$	0.27	$2.42{\cdot}10^{-2}$	0.64	3.98	9.71
u-square$_3$	$1.74{\cdot}10^{-2}$	16 325	45	$3.90{\cdot}10^{-1}$	0.21	$2.11{\cdot}10^{-2}$	0.38	6.55	14.57
u-square$_4$	$1.21{\cdot}10^{-2}$	32 636	46	$2.83{\cdot}10^{-1}$	0.93	$4.37{\cdot}10^{-3}$	4.55	7.86	17.20
u-square$_5$	$8.70{\cdot}10^{-3}$	65 297	59	$3.42{\cdot}10^{-1}$	-0.55	$1.28{\cdot}10^{-2}$	-3.10	9.12	20.26
u-square$_6$	$6.11{\cdot}10^{-3}$	130 532	67	$3.68{\cdot}10^{-1}$	-0.21	$1.36{\cdot}10^{-2}$	-0.18	10.45	23.07
u-square$_7$	$4.47{\cdot}10^{-3}$	261 135	84	$2.70{\cdot}10^{-1}$	0.90	$6.28{\cdot}10^{-3}$	2.24	11.19	25.58
u-square$_8$	$3.11{\cdot}10^{-3}$	522 236	100	$3.08{\cdot}10^{-1}$	-0.38	$7.09{\cdot}10^{-3}$	-0.35	12.48	28.08

Table 12: Example 4.6: computed errors and estimated convergence rates (random Voronoi meshes).

Mesh	h	N	It	e_{H^1}	ecr	e_{L^2}	ecr	C_1	C_2
square$_1$	$6.38{\cdot}10^{-2}$	5006	44	$5.38{\cdot}10^{-1}$	-	$3.32{\cdot}10^{-2}$	-	2.54	11.47
square$_2$	$4.34{\cdot}10^{-2}$	10 008	50	$5.37{\cdot}10^{-1}$	0.00	$3.10{\cdot}10^{-2}$	0.19	4.02	17.49
square$_3$	$3.47{\cdot}10^{-2}$	20 007	54	$5.74{\cdot}10^{-1}$	-0.19	$5.02{\cdot}10^{-2}$	-1.39	3.81	18.71
square$_4$	$2.41{\cdot}10^{-2}$	40 011	57	$3.93{\cdot}10^{-1}$	1.09	$8.67{\cdot}10^{-3}$	5.07	5.21	25.08
square$_5$	$1.73{\cdot}10^{-2}$	80 007	70	$4.38{\cdot}10^{-1}$	-0.31	$1.38{\cdot}10^{-2}$	-1.34	6.14	29.99
square$_6$	$1.14{\cdot}10^{-2}$	160 028	85	$4.53{\cdot}10^{-1}$	-0.10	$2.12{\cdot}10^{-2}$	-1.23	8.81	40.18
square$_7$	$8.86{\cdot}10^{-3}$	320 020	97	$3.13{\cdot}10^{-1}$	1.07	$7.97{\cdot}10^{-3}$	2.82	8.73	43.77
square$_8$	$6.25{\cdot}10^{-3}$	640 035	113	$3.07{\cdot}10^{-1}$	0.05	$6.11{\cdot}10^{-3}$	0.77	10.18	50.90

Acknowledgments

The authors are members of the INdAM Research group GNCS and this work is partially funded by INDAM-GNCS. P.F.A. and M.V. acknowledge the financial support of MIUR thourgh the PRIN grant n. 201744KLJL.

References

[1] D. Adak, E. Natarajan, and S. Kumar. Convergence analysis of virtual element methods for semilinear parabolic problems on polygonal meshes. *Numer. Methods Partial Differential Equations*, 35(1):222–245, 2019.

[2] D. Adak, E. Natarajan, and S. Kumar. Virtual element method for semilinear hyperbolic problems on polygonal meshes. *Int. J. Comput. Math.*, 96(5):971–991, 2019.

[3] D. Adak, S. Natarajan, and E. Natarajan. Virtual element method for semilinear elliptic problems on polygonal meshes. *Appl. Numer. Math.*, 145:175–187, 2019.

[4] P. F. Antonietti, L. Beirão da Veiga, S. Scacchi, and M. Verani. A $\mathcal{C}^1$ Virtual Element Method for the Cahn–Hilliard equation with polygonal meshes. *SIAM J. Numer. Anal.*, 54(1):34–56, 2016.

[5] E. Artioli, L. Beirão da Veiga, C. Lovadina, and E. Sacco. Arbitrary order 2D virtual elements for polygonal meshes: part II, inelastic problem. *Comput. Mech.*, 60(4):643–657, 2017.

[6] L. Beirão da Veiga and A. Ern. Preface [Special issue—Polyhedral discretization for PDE]. *ESAIM Math. Model. Numer. Anal.*, 50(3):633–634, 2016.

[7] L. Beirão da Veiga, C. Lovadina, and D. Mora. A virtual element method for elastic and inelastic problems on polytope meshes. *Comput. Methods Appl. Mech. Engrg.*, 295:327–346, 2015.

[8] L. Beirão da Veiga, C. Lovadina, and A. Russo. Stability analysis for the virtual element method. *Math. Models Methods Appl. Sci.*, 27(13):2557–2594, 2017.

[9] L. Beirão da Veiga, C. Lovadina, and G. Vacca. Virtual elements for the Navier-Stokes problem on polygonal meshes. *SIAM J. Numer. Anal.*, 56(3):1210–1242, 2018.

[10] L. Beirão da Veiga, F. Brezzi, A. Cangiani, G. Manzini, L. Marini, and A. Russo. Basic principles of Virtual Element Methods. *Mathematical Models and Methods in Applied Sciences*, 23(01):199–214, 2013.

[11] E. Cáceres, G. N. Gatica, and F. A. Sequeira. A mixed virtual element method for quasi-Newtonian Stokes flows. *SIAM J. Numer. Anal.*, 56(1):317–343, 2018.

[12] A. Cangiani, P. Chatzipantelidis, G. Diwan, and E. H. Georgoulis. Virtual element method for quasilinear elliptic problems. Technical report, arXiv:1707.01592, 2017.

[13] P. G. Ciarlet. *The finite element method for elliptic problems.* North-Holland Publishing Co., Amsterdam-New York-Oxford, 1978. Studies in Mathematics and its Applications, Vol. 4.

[14] P. Concus. Numerical solution of the minimal surface equation. *Math. Comp.*, 21:340–350, 1967.

[15] G. N. Gatica, M. Munar, and F. A. Sequeira. A mixed virtual element method for a nonlinear Brinkman model of porous media flow. *Calcolo*, 55(2):Art. 21, 36, 2018.

[16] C. Johnson and V. Thomée. Error estimates for a finite element approximation of a minimal surface. *Math. Comp.*, 29:343–349, 1975.

[17] X. Liu and Z. Chen. A virtual element method for the Cahn-Hilliard problem in mixed form. *Appl. Math. Lett.*, 87:115–124, 2019.

[18] J. C. C. Nitsche. On new results in the theory of minimal surfaces. *Bull. Amer. Math. Soc.*, 71:195–270, 1965.

[19] O. Trasdahl and E. M. Ronquist. High order numerical approximation of minimal surfaces. *J. Comput. Phys.*, 230(12):4795–4810, 2011.

[20] F. Wang and H. Wei. Virtual element methods for the obstacle problem. *IMA J. Numer. Anal.*, 10.1093/imanum/dry055, 2018.